# Theoretical study on neutron distribution of $^{208}$Pb by parity-violating electron scattering*

Jian Liu(刘健)[1,2;1)] Cun Zhang(张存)[2] Zhong-Zhou Ren(任中洲)[2,3,4] Chang Xu(许昌)[2]

[1] College of Science, China University of Petroleum (East China), Qingdao 266580, China
[2] School of Physics and Key Laboratory of Modern Acoustics, Institute of Acoustics, Nanjing University, Nanjing 210093, China
[3] Kavli Institute for Theoretical Physics China, Beijing 100190, China
[4] Center of Theoretical Nuclear Physics, National Laboratory of Heavy-Ion Accelerator, Lanzhou 730000, China

**Abstract:** The precise determination of neutron distribution has important implications for both nuclear structure and nuclear astrophysics. The purpose of this paper is to study the characteristics of neutron distribution of $^{208}$Pb by parity-violating electron scattering (PVS). Parity-violating asymmetries of $^{208}$Pb with different types of neutron skins are systematically calculated and compared with the experimental data of PREx. The results indicate that the PVS experiments are very sensitive to the nuclear neutron distributions. From further PVS measurements, detailed information on nuclear neutron distributions can be extracted.

**Keywords:** parity-violating electron scattering, nuclear neutron distributions, neutron and proton form factors

**PACS:** 21.10.Gv, 24.80.+y, 25.30.Bf **DOI:** 10.1088/1674-1137/40/3/034101

## 1 Introduction

The determination of size and shape of nuclei is a basic but important part of nuclear physics research. During the past several decades, the charge densities of stable and long-lived nuclei have been accurately measured by high-energy electron scattering [1–3]. However, the determination of nuclear neutron distributions has been an open issue for a long period of time. The uncertainty of the nuclear neutron skin ($R_{\rm skin} \equiv R_{\rm n} - R_{\rm p}$) leaves the isovector interaction in nuclear structure models undetermined. Different force parameter sets often lead to different neutron radii when describing the same nucleus [4–9].

Compared with hadronic probes, electronic probes have considerable advantages in neutron skin measurements. The interaction between the electron and the nucleus is well understood and the probing can cover the whole nuclear volume [10, 11]. With some mild assumptions on the relation between $A_{\rm pv}$ and $R_{\rm n}$ [12–15], the PREx collaboration extracted the neutron skin of $^{208}$Pb: $R_{\rm skin} = 0.33^{+0.16}_{-0.18}$ fm [16, 17] by parity-violating electron scattering. Besides the PREx experiment, an experiment on coherent $\pi^0$ photoproduction has been carried out at Mainz very recently and extracted $R_{\rm skin}$ of $^{208}$Pb to be $0.15 \pm 0.03({\rm stat.})^{+0.01}_{-0.03}({\rm sys.})$ fm [18].

The nuclear neutron skins only provide a simple description of the nuclear neutron properties, because the same root-mean-square (RMS) radius can correspond to different density distributions. An accurate description of the nuclear proton and neutron densities is important because many properties of nuclei are closely related to the surface diffuseness, such as the nuclear Coulomb barrier and fusion of heavy-ions [19, 20]. For stable nuclei, the extracted proton density distributions can be described by the two-parameter Fermi (2pF) model: $\rho_{\rm p} = \rho_0/\{1+\exp[(r-C_{\rm p})/a_{\rm p})]\}$, where $C_{\rm p}$ is the half density radius and $a_{\rm p}$ is the diffuseness parameter. In Refs. [18, 21], $C_{\rm p}$ and $a_{\rm p}$ were determined to be 6.680 fm and 0.447 fm respectively for $^{208}$Pb. A reanalysis of the experimental data recently suggested the 2pF parameters of proton density of $^{208}$Pb should be $C_{\rm p} = 6.613(40)$ fm and $a_{\rm p} = 0.497(20)$ fm [22].

Compared with the nuclear proton densities, it is much more difficult to measure the neutron density distributions and fewer experimental results are available. The antiprotonic atom experiments have shown that in $^{208}$Pb the neutron density distribution is close to the "halo-type" which is $C_{\rm n} = C_{\rm p}$ and $a_{\rm n} > a_{\rm p}$ [23, 24], where $C_{\rm n}$ and $a_{\rm n}$ are the half density radius and the diffuseness parameter respectively for neutron density distributions. On the other hand, if $C_{\rm n} > C_{\rm p}$ and $a_{\rm n} = a_{\rm p}$,

Received 18 June 2015

∗ Supported by the National Natural Science Foundation of China (11505292, 11175085, 11235001, 11447226), by the Shandong Provincial Natural Science Foundation, China (BS2014SF007), by the Fundamental Research Funds for the Central Universities (15CX02072A, 15CX02070A, 15CX05026A, 13CX10022A, 14CX02157A).

1) E-mail: liujian@upc.edu.cn

this type of neutron density is referred to as the neutron "skin-type" distribution. Besides the antiprotonic atom experiments, the recent coherent pion photoproduction experiment also indicates that the neutron distribution of $^{208}$Pb has a halo character, with $C_{\rm n}$ and $a_{\rm n}$ determined to be 6.70±0.03(stat.) fm and 0.55±0.01(stat.)$^{+0.02}_{-0.03}$(sys.) fm, respectively [18].

Besides the experimental measurements, the parameters of nuclear neutron distributions are also extracted from the mean-field calculations and the origin of the neutron skin has been investigated theoretically in many previous works [21, 25, 26]. It can be found that nuclear models with soft symmetry energies always predict the neutron skin of $^{208}$Pb to be close to the halo-type, for example $\Delta C_{\rm np}=-0.04$ fm for HFB-8, $\Delta C_{\rm np}=0.03$ fm for D1S, and $\Delta C_{\rm np}=0.05$ fm for DD-ME2 [25]. For mean-field interactions with stiff symmetry energies, the models always lead to a mixed-type neutron distribution ($\Delta C_{\rm np}>0, \Delta a_{\rm np}>0$) for $^{208}$Pb. Though the theoretical nuclear model can well describe many nuclear properties, such as the binding energies and charge distributions, there are still large uncertainties on the theoretical results of $\Delta C_{\rm np}$ and $\Delta a_{\rm np}$, which are worthy of further research.

In this paper, we systematically investigate the neutron density distribution of $^{208}$Pb by parity-violating electron scattering. First, the parity-violating asymmetries of $^{208}$Pb are calculated and compared with the experimental data of PREx where the corresponding neutron distributions are taken as the halo- and skin-type, respectively. Then, the sensitivity of $A_{\rm pv}$ to parameters of neutron distributions is further investigated for two types of neutron distribution. Through calculation one can see that the parity-violating electron scattering is more sensitive to the half density radius $C_{\rm n}$ because the probing covers the whole nuclear volume. Furthermore, comparative studies are made on parity-violating electron scattering for two types of neutron density distribution by investigating the corresponding form factors. From analysis with the 2pF and Helm models, it can be found that the parity-violating asymmetries are closely connected to the corresponding neutron and proton form factors. Small changes of different parameters in the modeled neutron distributions can lead to very different changes of $A_{\rm pv}$, which can be used to identify the characteristics of nuclear neutron distributions from PVS experiments.

The paper is organized as follows. In Sec. 2 we present the theoretical framework of parity-violating electron scattering off nuclei. In Sec. 3 we analyze the numerical results. Finally, a summary is given in Sec. 4.

## 2 Theoretical framework

In this section, the main formula of parity-violating electron scattering is outlined. Parity-violating electron scattering (PVS) is considered to be a model-independent method to probe the nuclear neutron properties, and was first proposed in 1989 [27]. During the scattering process, the incident longitudinally polarized electrons interact with nucleons by exchanging either a photon or a $Z^0$ boson and the $Z^0$ boson couples primarily to neutrons, which leads to the parity-violating experiment being sensitive to the neutron distribution [27]. The parity-violating asymmetry $A_{\rm pv}$, which originates from the interference between the electromagnetic and electroweak amplitudes, is defined as the difference between the cross sections of left and right helicity electrons [10]:

$$A_{\rm pv}=\frac{{\rm d}\sigma_+-{\rm d}\sigma_-}{{\rm d}\sigma_++{\rm d}\sigma_-}=\frac{2{\rm Re}[M_\gamma^* M_Z]}{|M_\gamma|^2}, \tag{1}$$

where $M_\gamma$ is the electromagnetic amplitude and $M_Z$ is the electroweak amplitude.

### 2.1 Plane wave Born approximation

For the $J_\pi=0^+$ target, the electromagnetic and weak amplitudes in Eq. (1) are simply replaced by the nuclear charge and weak charge form factors in the plane wave Born approximation (PWBA). The parity-violating asymmetry $A_{\rm pv}$ can be written as:

$$A_{\rm pv}=\frac{G_{\rm F}q^2}{4\pi\alpha\sqrt{2}}\frac{Q_{\rm wk}\cdot F_{\rm wk}(q)}{Z\cdot F_{\rm ch}(q)}, \tag{2}$$

where $\alpha$ is the fine structure constant and $G_{\rm F}=1.16639\times 10^{-5}{\rm GeV}^{-2}$ is the Fermi constant. $Q_{\rm wk}$ is the weak-charge number of the nucleus which can be obtained by $Q_{\rm wk}=g_{\rm v}^{\rm p}Z+g_{\rm v}^{\rm n}N$ ($g_{\rm v}^{\rm p}\approx 0.0712$, $g_{\rm v}^{\rm n}\approx -0.9877$). $F_{\rm wk}(q)$ and $F_{\rm ch}(q)$ are the weak-charge and charge form factors, respectively, which contain the detailed information of the nuclear structure:

$$F_{\rm ch}(q)=G_{\rm E}^{\rm p}(q)F_{\rm p}(q)+\frac{N}{Z}G_{\rm E}^{\rm n}(q)F_{\rm n}(q), \tag{3}$$

$$\begin{aligned}F_{\rm wk}(q)=&G_{\rm E}^{\rm p}(q)\left[F_{\rm n}(q)-\frac{Z}{N}(1-4\sin^2\theta_{\rm W})F_{\rm p}(q)\right]\\&-G_{\rm E}^{\rm n}(q)\left[F_{\rm n}(q)(1-4\sin^2\theta_{\rm W})-\frac{Z}{N}F_{\rm p}(q)\right],\end{aligned} \tag{4}$$

where $G_{\rm E}^{\rm p}(q)$ and $G_{\rm E}^{\rm n}(q)$ are the electromagnetic single-nucleon form factors [28], $\sin^2\theta_{\rm W}=0.23$ is the Weinberg angle, $F_{\rm p}(q)$ and $F_{\rm n}(q)$ are the form factors of point proton and neutron density distribution, respectively. Compared with $G_{\rm E}^{\rm p}(q)$, the charge form factor of the neutron $G_{\rm E}^{\rm n}(q)$ can be neglected for small momentum transfers. Substituting Eqs. (3) into Eq. (2), the parity-violating asymmetry $A_{\rm pv}$ in PWBA can be rewritten as:

$$A_{\rm pv}=\frac{G_{\rm F}q^2Q_{\rm wk}}{4\pi\alpha\sqrt{2}Z}\left[\frac{F_{\rm n}(q)}{F_{\rm p}(q)}-\frac{Z}{N}(1-4\sin^2\theta_{\rm W})\right]. \quad (5)$$

Eq. (4) has a compact structure and is convenient for the physical analysis. It connects $A_{\rm pv}$ with the nuclear proton and neutron form factors in a direct way; however, the Coulomb distortion corrections to the wave functions of scattering electrons are not included in this formula. For electron scattering off heavy nuclei, the Coulomb distortion effects modify the wave functions of scattering electrons significantly and needs to be taken into account during the calculations [29].

### 2.2 Phase-shift analysis method

There are multiple ways to include the Coulomb distortion effects of heavy nuclei during the studies of PVS and the phase-shift analysis method is one of the convenient methods. It is also referred to as the distorted wave Born approximation (DWBA). For the phase-shift analysis method, the Coulomb distortion effects are included in Eq. (1) by solving the Dirac equation of the left and right helicity electrons with the phase-shift analysis method [30]:

$$\left[\vec{\alpha}\cdot\vec{p}+\beta m_{\rm e}+\hat{V}(r)\right]\Psi=E\Psi. \quad (6)$$

The total potential $\hat{V}(r)$ in Eq. (6) consists of two parts, the vector Coulomb potential $V(r)$ and axial vector weak potential $A(r)$:

$$\hat{V}(r)=V_{\rm C}(r)+\gamma_5 A(r). \quad (7)$$

The solution of the Dirac equation Eq. (6) can be decomposed into different partial waves with definite orbital angular momentum and spin orientation. The cross sections of different helicity electrons can be calculated as follows:

$$\frac{{\rm d}\sigma}{{\rm d}\Omega}=|f(\theta)|^2+|g(\theta)|^2, \quad (8)$$

where the direct scattering amplitude $f(\theta)$ and spin-flip scattering amplitude $g(\theta)$ can be determined by the phase shifts of different partial waves:

$$f(\theta)=\frac{1}{2ik}\sum_{l=0}^{\infty}\left[(l+1)(e^{2i\delta_l^+}-1)+(e^{2i\delta_l^-}-1)\right]P_l(\cos\theta),$$
$$g(\theta)=\frac{1}{2ik}\sum_{l=0}^{\infty}\left[e^{2i\delta_l^-}-e^{2i\delta_l^+}\right]P_l^1(\cos\theta), \quad (9)$$

with $P_l$ and $P_l^1$ denoting the Legendre and associated Legendre function. By solving the Dirac Eq. (6) with the phase-shift analysis method, the cross sections of different helicity electrons $\sigma_\pm$ can be accurately calculated. Substituting $\sigma_\pm$ into Eq. (1), the parity-violating asymmetry $A_{\rm pv}$ can be obtained. The Coulomb distortion corrections are taken into account by including the Coulomb potential in Eq. (7) during the solution of Dirac equation Eq. (6).

## 3 Numerical results and analysis

As already mentioned in the introduction, the neutron density distribution of $^{208}$Pb displays a halo character in both the antiprotonic atom experiments [23, 24] and the coherent pion photoproduction experiment [18]. It is known to us that parity-violating electron scattering is also an effective method to probe the nuclear neutron properties. Therefore, in this section, parity-violating electron scattering off $^{208}$Pb is studied with the formulas of Sec. 2.

### 3.1 $A_{\rm pv}$ at kinematics of PREx

Firstly, the parity-violating asymmetries $A_{\rm pv}$ of $^{208}$Pb at the kinematics of PREx are calculated with the phase-shift analysis method and the results are compared with the experimental data in Fig. 1. During the investigation, the 2pF proton density in Ref. [22] ($C_{\rm p}=6.613(40)$ fm and $a_{\rm p}=0.497(20)$ fm) is used. For nuclear neutron density, two types of distributions are taken: (a) neutron halo-type distribution $C_{\rm n}=C_{\rm p}$, $a_{\rm n}>a_{\rm p}$; (b) neutron skin-type distribution $C_{\rm n}>C_{\rm p}$, $a_{\rm n}=a_{\rm p}$. The neutron skin thickness of $^{208}$Pb is taken to be 0.33 fm, which is the experimental result of PREx. Besides, the theoretical $A_{\rm pv}$ for the extreme neutron density distribution ($\Delta C_{\rm np}=0$ and $\Delta a_{\rm np}=0$) is also calculated and presented in Fig. 1 as a control. One can see that there are significant deviations between the experimental data and theoretical $A_{\rm pv}$ from the extreme neutron distribution ($\Delta C_{\rm np}=0$ and $\Delta a_{\rm np}=0$).

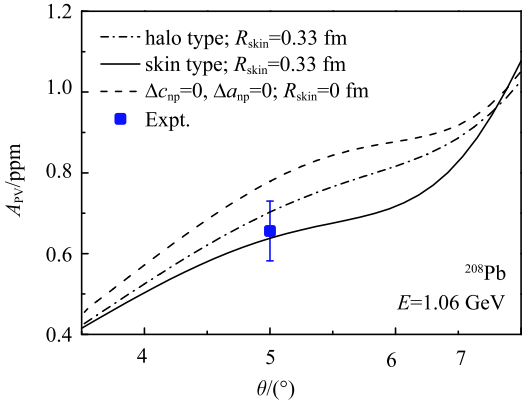


Fig. 1. (color online) $A_{\rm pv}$ of $^{208}$Pb for different types of neutron distributions at the kinematics of PREx. The blue square is the experimental $A_{\rm pv}$ of PREx.

If we suppose that $R_{\rm skin}=0.33$ fm and neutron density distribution has a skin character ($\Delta C_{\rm np}>0$ and $\Delta a_{\rm np}=0$), the theoretical result coincides with the experimental data very well in Fig. 1. Assuming that $R_{\rm skin}=0.33$ fm and $R_{\rm skin}$ is only due to the increase of neutron surface diffuseness ($\Delta C_{\rm np}=0$ and $\Delta a_{\rm np}>0$), the theoretical $A_{\rm pv}$ is also compatible with the experimental data of PREx within one standard deviation. From the previous theoretical analysis, the nuclear models with soft symmetry energies always predict the neutron skin of $^{208}$Pb close to the halo-type and the mean-field interactions with stiff symmetry energies always lead to a mixed-type neutron distribution ($\Delta C_{\rm np}>0, \Delta a_{\rm np}>0$) for $^{208}$Pb [25]. It can be seen in Fig. 2 that the character of the neutron skin of $^{208}$Pb cannot be determined from the PVS experiment at present, because there is only one experimental measurement and the error bar is large. Now, a second measurement of $^{208}$Pb called PREx-II is in progress whose proposed error is one third of the present value [31, 32]. From the results of the new experiment, our understanding of the neutron distribution will be further improved. From Fig. 1, one can also find that the $A_{\rm pv}$ is sensitive to the changes of half density radius $C_{\rm n}$ rather than the surface diffuseness $a_{\rm n}$. The sensitivities of $A_{\rm pv}$ to parameters of neutron distributions are further discussed in the following sections.

### 3.2 Statistical errors for measuring $C_{\rm n}$ and $a_{\rm n}$ in PVS experiments

Studying the extraction of neutron density distributions from the experiments, it is important for the theoretical evaluations coming with estimations of corresponding theoretical uncertainties [26, 33, 34]. For PVS experiments, two measurements at different momentum transfers are needed to constrain the parameters of density distributions, if the neutron densities are described by the 2pF model [13, 14]. In this part, the statistical errors for measuring half density radius $C_{\rm n}$ and diffuseness parameter $a_{\rm n}$ in PVS experiments are contrasted with each other for two types of neutron distributions.

With the $R_{\rm skin}$ of nuclei fixed by an earlier PVS measurement, the statistical errors for measuring parameters $C_{\rm n}$ and $a_{\rm n}$ can be calculated with the formula [13]:

$$\frac{\Delta X}{X}=\frac{1}{\sqrt{N_{\rm tot}}A_{\rm pv}P\epsilon_X}, \tag{10}$$

where $X$ represents the half density radius $C_{\rm n}$ or the diffuseness parameter $a_{\rm n}$. $P$ is the beam polarization and $N_{\rm tot}$ is the total number of electrons detected during a running time $T$ [31]. $\epsilon_X$ in Eq. (10) is the sensitivity of $A_{\rm pv}$ to parameter $X$, which is defined as:

$$\epsilon_X=\frac{{\rm d}\ln A_{\rm pv}}{{\rm d}\ln X}=\frac{X}{A_{\rm pv}}\cdot\frac{{\rm d}A_{\rm pv}}{{\rm d}X}. \tag{11}$$

Statistical errors for measuring $C_{\rm n}$ and $a_{\rm n}$ of 2pF neutron distributions of $^{208}$Pb are investigated with Eqs. (10) and (11) at the kinematics of PREx and the results are presented in Fig. 2. It can be seen from this figure that the statistical errors for measuring $C_{\rm n}$ in PVS experiments are much smaller than those for measuring $a_{\rm n}$. This is because the measurements of PVS experiments cover the whole nuclear volume. The overall neutron distributions of nuclei have a much greater impact on PVS than those in the periphery of the nuclei, which makes the PVS experiments more sensitive to the half density radius $C_{\rm n}$ than the surface diffuseness $a_{\rm n}$.

It can also be seen in the two panels of Fig. 2 that the statistical errors for measuring $C_{\rm n}$ and $a_{\rm n}$ have similar variation trends with the scattering angle. No matter which type the neutron distribution is, the statistical errors for measuring $C_{\rm n}$ and $a_{\rm n}$ of $^{208}$Pb are relatively small at the scattering angles 5° and 8°. The measurement at 5° has been carried out at PREx and $R_{\rm skin}$ of $^{208}$Pb is extracted according to its experimental data. If a further PVS measurement is carried out at 8°, the parameter $C_{\rm n}$ of 2pF neutron distribution of $^{208}$Pb can be determined

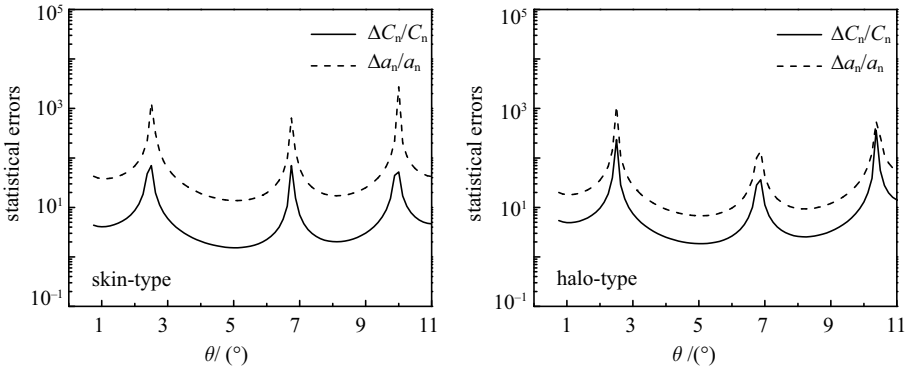


Fig. 2. Statistical errors of PVS experiments for measuring $C_{\rm n}$ and $a_{\rm n}$ of $^{208}$Pb in 30 days at the kinematics of PREx. The neutron distributions in the left and right panels are assumed to be the skin- and halo-type, respectively.

with relatively small statistical errors. Combining with other experiments which are sensitive to the surface diffuseness $a_{\rm n}$, detailed information on the nuclear neutron distributions can be extracted.

### 3.3 Contrast analysis on PVS using the 2pF and Helm model

From the previous discussion, one can find that the parity-violating electron scattering is sensitive to the nuclear neutron distributions. In this part further comparative studies are made on parity-violating electron scattering for halo- and skin-types of neutron density distributions. In this way, the influences of different parameters in modeled neutron distributions on parity-violating electron scattering can be analyzed. Different modeled neutron density distributions are taken into consideration during the investigations. It is useful for us to study electron scattering with some modeled density distributions because the parameters in modeled densities are closely related to the nuclear density distributions in the bulk and surface regions [35, 36].

Firstly, we assume that the proton and neutron densities of $^{208}$Pb are the 2pF profiles and investigate the parity-violating electron scattering for halo- and skin-type neutron distributions, respectively. The results are presented in Fig. 3. During the calculation, the neutron skin thickness of $^{208}$Pb is taken to be $R_{\rm skin} = 0.33$ fm and the 2pF proton density distribution in Ref. [22] is used. From Fig. 3(a), one can see that for the halo-type neutron distribution, $A_{\rm pv}$ increases moderately with the scattering angle; however for the skin-type one, $A_{\rm pv}$ has a much larger amplitude. There are significant differences between the parity-violating asymmetries $A_{\rm pv}$ for two types of neutron density distribution, even in the range of small scattering angles in Fig. 1. These differences can be used to identify the characteristics of nuclear neutron distribution by the PVS experiments.

The differences for the two types of neutron distributions in Fig. 3(a) can be interpreted with the PWBA method. In Eq. (4), when the zero points of neutron and proton form factors are located at different positions, the amplitudes of $A_{\rm pv}$ will be infinite. Taking into account the Coulomb distortions during the calculation, the values of $A_{\rm pv}$ are finite. In Fig. 3(b) and Fig. 3(c) we present the corresponding neutron and proton form factors for two types of neutron distribution. One can see that for the skin-type neutron density distribution, the minima of $F_{\rm n}(q)$ and $F_{\rm p}(q)$ are located at different momentum transfers. For the halo-type one, the minima of $F_{\rm n}(q)$ and $F_{\rm p}(q)$ are located at almost the same positions but the values of $F_{\rm n}(q)$ are smaller than those of $F_{\rm p}(q)$. Substituting $F_{\rm n}(q)$ and $F_{\rm p}(q)$ into Eq. (4), the differences of $A_{\rm pv}$ between halo- and skin-type neutron distributions can be interpreted with the PWBA method.

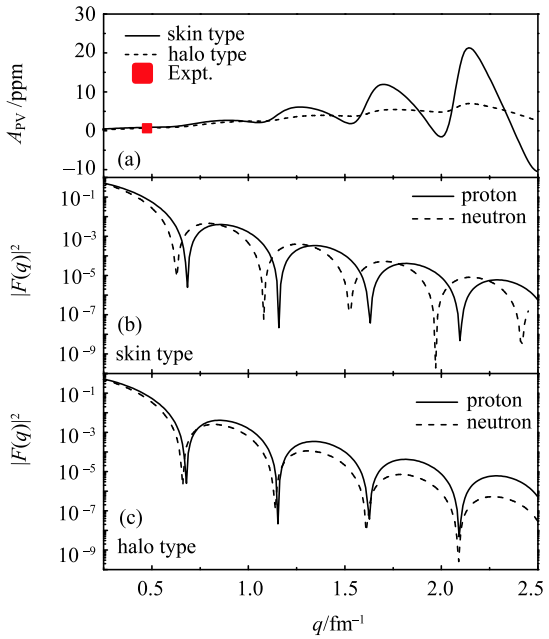


Fig. 3. (color online) Contrast analysis of PVS with the 2pF model. (a) $A_{\rm pv}$ of $^{208}$Pb for halo- and skin-type neutron distributions at the kinematics of PREx. (b) form factors for the skin-type neutron distribution. (c) form factors for the halo-type neutron distribution.

Besides the 2pF model, parity-violating electron scattering off nuclei are also investigated with the Helm model for its good analytical properties. The Helm model density distribution is defined as the convolution of a constant density $\rho_0$ in a hard sphere of radius $R_0$ (the diffraction radius) with a Gaussian distribution of variance $\sigma^2$ [37]:

$$\rho^{\rm H}(r) = \int {\rm d}\vec{\boldsymbol{r}}' f_{\rm G}(\vec{\boldsymbol{r}} - \vec{\boldsymbol{r}}')\rho_0 \Theta(R_0 - r), \tag{12}$$

where $f_{\rm G}(r) = (2\pi\sigma^2)^{-3/2}{\rm e}^{-r^2/2\sigma^2}$. The form factors of Helm model distributions can be obtained analytically:

$$F^{\rm H}(q) = \frac{3}{qR_0} j_1(qR_0){\rm e}^{-\sigma^2 q^2/2}, \tag{13}$$

where $j_1(x)$ is the spherical Bessel function. The diffraction radius $R_0$ in Eq. (12) characterizes the size of the density distribution and the diffuseness parameter $\sigma$ describes the thickness of the surface. For the Helm model proton density of $^{208}$Pb, we extract $R_{0\rm p} = 6.797$ fm and $\sigma_{\rm p} = 0.913$ fm from the experimental charge density distribution.

In the Helm model, one can also define the neutron skin-type distribution: $R_{0\rm n} > R_{0\rm p}$, $\sigma_{\rm n} = \sigma_{\rm p}$ and the neutron halo-type distribution: $R_{0\rm n} = R_{0\rm p}$, $\sigma_{\rm n} > \sigma_{\rm p}$. The parity-violating asymmetries of $^{208}$Pb for two types of neutron distributions in Helm models are calculated and

presented in Fig. 4(a). Similar to Fig. 3, the amplitudes of $A_{\rm pv}$ for the skin-type neutron distribution are much larger than those for the halo-type one. $F_{\rm n}(q)$ and $F_{\rm p}(q)$ for the Helm model density profiles of $^{208}$Pb are also calculated by Eq. (13) and presented in Fig. 4(b) and Fig. 4(c). In Eq. (13), the positions of minima of form factors are determined by the diffraction radius $R_0$ and the attenuation of form factors are determined by the diffuseness parameter $\sigma$. It can be seen again in the Helm models that the distances between the minima of $F_{\rm n}(q)$ and $F_{\rm p}(q)$ correspond to the amplitudes of $A_{\rm pv}$. For halo-type neutron distributions, the minima of $F_{\rm n}(q)$ and $F_{\rm p}(q)$ are at the same positions but $F_{\rm n}(q)$ falls much more rapidly than $F_{\rm p}(q)$, which leads to the very small $A_{\rm pv}$.

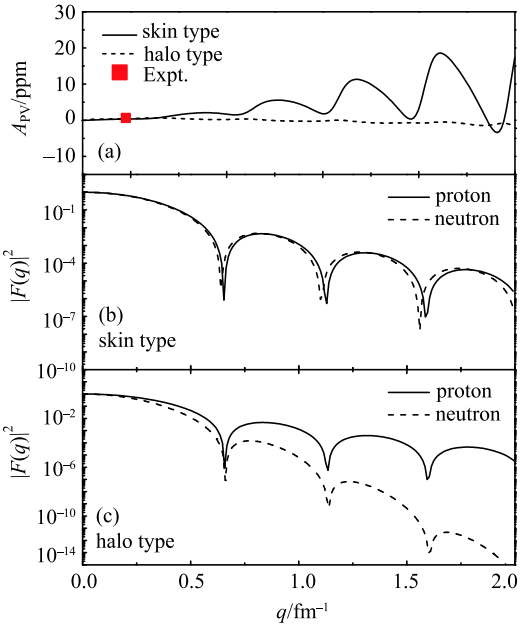


Fig. 4. (color online) Contrast analysis of PVS with the Helm model. (a) $A_{\rm pv}$ of $^{208}$Pb for halo- and skin-type neutron distributions at the kinematics of PREx. (b) form factors for the skin-type neutron distribution. (c) form factors for the halo-type one.

Combining the analysis of Figs. 3 and 4, it can be found that in the modeled density profiles, the half density radii affect the positions of minima of the form factors while the diffuseness parameters affect the attenuation degree of the form factors. Because $A_{\rm pv}$ of nuclei are closely linked with the nuclear form factors, the small variation of different parameters in the modeled neutron distributions can lead to very different changes of $A_{\rm pv}$. This can be used to identify the characteristics of nuclear neutron distributions from PVS experiments.

## 4 Summary

In this paper, the parity-violating electron scattering of $^{208}$Pb for halo- and skin-type neutron density distributions is systematically investigated. The theoretical results are compared with experimental data of PREx. One can see that $A_{\rm pv}$ for two types of neutron distribution are all compatible with the experimental data of PREx within one standard deviation. In order to extract the nuclear neutron distributions, further measurements with smaller error bars are needed. Besides, there are significant differences between the results of the two types of neutron distribution, which means that parity-violating electron scattering is sensitive to the neutron distribution.

The statistical errors for measuring $C_{\rm n}$ and $a_{\rm n}$ are further investigated for two types of neutron distribution. It is found that the statistical errors for measuring $C_{\rm n}$ are smaller than those of $a_{\rm n}$. This is due to the probing of electron scattering experiments covers the whole nuclear volume, which is an advantage of electron scattering. By parity-violating electron scattering, the diffraction radii of neutron distributions can be determined with a relatively small statistical error. Combining with other experiments which are sensitive to the nuclear surface diffuseness, detailed information on nuclear neutron density distributions can be extracted.

Comparative studies are also made on parity-violating electron scattering for two types of neutron density distribution by investigating the corresponding form factors. From analysis with the 2pF and Helm models, one can see that the diffraction radii determine the positions of the minima of form factors while the diffuseness parameters determine the attenuation of the form factors. The $A_{\rm pv}$ of nuclei are closely linked with the nuclear form factors and influenced to a large extent by the parameters of the modeled nuclear densities. Small changes of different parameters of neutron distributions can lead to large changes of $A_{\rm pv}$ and this allows PVS experiments to be used to identify the type of nuclear neutron distribution in stable long-lived nuclei.

## References


1 I. Angeli, At. Data Nucl. Data Tables, **87**: 185 2004.
2 H. De Vries, C. De Jager, W., C. De Vries, At. Data Nucl. Data Tables, 1987, **36**: 495.
3 I. Angeli, K. P. Marinova, At. Data Nucl. Data Tables, **99**: 69 (2013)
4 B. Brown, Phys. Rev. Lett., **85**: 5296 (2000)
5 B. G. Todd-Rutel, J. Piekarewicz, Phys. Rev. Lett., **95**: 122501 (2005)
6 G. A. Lalazissis, S. Karatzikos, R. Fossion, D. P. Arteaga, A. V. Afanasjev, P. Ring, Phys. Lett. B, **671**: 36 (2009)
7 M. Centelles, X. Roca-Maza, X. Viñas, M. Warda, Phys. Rev. Lett., **102**: 122502 (2009)
8 F. J. Fattoyev, C. J. Horowitz, J. Piekarewicz, G. SHEN, Phys. Rev. C, **82**: 055803 (2010)
9 W. C.CHEN, J. Piekarewicz, Phys. Rev. C, **90**: 044305 (2014)
10 R. González-Jiménez, J. A. Caballero, T. W. Donnelly, Phys. Rep. **524**: 1 (2013)
11 Y. J. CHEN, Chin. Phys. C, **37**: 074101 (2013)
12 X. Roca-Maza, M. Centelles, X. Viñas, M. Warda, Phys. Rev. Lett. **106**: 252501 (2011)
13 S. BAN, C. J. Horowitz, R. Michaels, J. Phys. G, **39**: 015104 (2012)
14 J. LIU, Z. Z. REN, T. K. DONG, Nucl. Phys. A, **888**: 45 (2012)
15 P. G. Reinhard, J. Piekarewicz, W. Nazarewicz, B. K. Agrawal, N. Paar, X. Roca-Maza, Phys. Rev. C, **88**: 034325 (2013)
16 S. Abrahamyan, et al., Phys. Rev. Lett. **108**: 112502 (2012)
17 C. J. Horowitz, et al., Phys. Rev. C, **85**: 032501(R) (2012)
18 C. M. Tarbert, et al., Phys. Rev. Lett. **112**: 242502 (2014)
19 I. Dutt, R. Puri, Phys. Rev. C, **81**: 047601 (2010)
20 G. G. Adamian, N. V. Antonenko, L. A. Malov, G. Scamps, D. Lacroix , Phys. Rev. C, **90**: 034322 (2014)
21 M. Warda, X. Viñas, X. Roca-Maza, M. Centelles, Phys. Rev. C, **81**: 054309 (2010)
22 A. B. Jones, B. A. Brown, Phys. Rev. C, **90**: 067304 (2014)
23 B. Kłos, et al., Phys. Rev. C, **76**: 014311 (2007)
24 A. Trzcińska, J. Jastrzębski, P. Lubiński, F. J. Hartmann, R. Schmidt, von T. Egidy, B. Kłos, Phys. Rev. Lett. **87**: 082501 (2001)
25 M. Centelles, X. Roca-Maza, X. Viñas, M. Warda, Phys. Rev. C, **82**: 054314 (2010)
26 J. LIU, Z. Z. REN, C. XU, R. L. XU, Phys. Rev. C, **88**: 054321 (2013)
27 T. W. Donnelly, J. Dubach, I. Sick, Nucl. Phys. A, **503**: 589 (1989)
28 C. J. Horowitz, J. Piekarewicz, Phys. Rev. C, **86**: 045503 (2012)
29 D. H. Jakubassa-Amundsen, J. Phys. G, **41**: 075103 (2014)
30 C. J. Horowitz, Phys. Rev. C, **57**: 3430 (1998)
31 P. Souder et al., PREX-II Proposal. 2012.[http://hallaweb.jlab.org/parity/prex].
32 S. Riordan et al., C-REX Proposal. 2013.[http://hallaweb.jlab.org/parity/prex].
33 O. Moreno, T. W. Donnelly, Phys. Rev. C, **89**: 015501 (2014)
34 O. Moreno, T. W. Donnelly, J. Phys. G, **42**: 034006 (2015)
35 X. Roca-Maza, M. Centelles, F. Salvat, X. Viñas, Phys. Rev. C, **87**: 014304 (2013)
36 N. Warda, M. Centelles, X. Viñas, X. Roca-Maza, Phys. Rev. C, **89**: 064302 (2014)
37 D. Sprung, N. Yamanishi, D. C. ZHENG, Nucl. Phys. A, **550**: 89 (1992)